Epitaxy and Structure of Paraffin–Diluent Eutectics

Douglas L. Dorset,* James Hanlon, and Gail Karet

Electron Diffraction Department, Medical Foundation of Buffalo, Inc., 73 High Street, Buffalo, New York 14203. *Received July 27, 1988; Revised Manuscript Received November 29, 1988*

ABSTRACT: Because of the demonstrated importance of certain diluents as agents for epitaxially orienting polymethylene chain compounds, the respective eutectic solids between the paraffin *n*-hexatriacontane and naphthalene, anthracene, acridine, and benzoic acid are studied by calorimetric, optical, and diffraction techniques to understand the optimal conditions for coupled crystal growth. Of the four eutectics, only those solely involving nonpolar molecules can be described by the Schröder equation. The liquidus curve for paraffin–benzoic acid eutectics is reasonably well fit by nonideal theory; the eutectic with acridine is complicated since this material crystallizes in several polymorphic forms.

Introduction

As stated by Copley,[1] the existence of a eutectic solid in itself infers little about its structure, except that it is presumed to be some intimate mixture of two components (pure compounds or solid solutions). Although this mixture is sometimes[2] stated to be "mechanical", implying that the constituent materials can be physically separated, there are enough data on many types of eutectics, including metallic alloys, which indicate the presence of rather tight interfacial interactions, leading to high-strength materials.[3]

The study of surface interactions between constituents of eutectic solids has been a major activity in metallurgical research, sometimes leading to the use of organic materials as optically transparent models for various types of binary metal solids.[4-7] From such studies, three types of eutectic structures have been proposed by Hunt and Jackson,[4] and the existence of each is though to be controlled largely by the diffusibility and/or interphase interaction energy of individual components crystallizing from the molten solution. When diffusion of the two components is favorable, a *nonfaceted–nonfaceted* eutectic solid is formed which can be lamellar or rodlike. That cooperative interactions of the two materials are involved in this coupled crystal growth was also demonstrated by Podolinskii.[6] When this coupled crystallization is limited by either diffusion or interfacial interactions, the solid is termed a *nonfaceted–faceted type*, which nevertheless can yield a lamellar eutectic solid. Podolinskii[6] demonstrated that the interaction of naphthalene with phenanthrene can form this structure. Finally, when no coupled interaction is possible, an anomalous or *faceted–faceted* structure is formed. One expression of this is when the growth front between two component materials allows no surface adsorption to occur.[6] It is obvious that epitaxy must play some role in the interaction of some materials, as illustrated by the specific surface nucleation in lamellar metallic eutectic solids.[3]

Application of these principles to polymer–diluent systems can be found in the extensive work of Smith and Pennings.[8-12] In general the texture of the eutectic solid was found to be dependent upon the cooling rate was well as the mole fraction of constituent in the melt. In many cases there was evidence for a specific interaction between the polymer and diluent crystals—e.g., in nonfaceted–faceted eutectic growth—within certain concentration ranges. Although this was not explicitly shown in this early work, the implied epitaxial relationship for some polymer–diluent combinations was directly demonstrated by Wittmann and Manley[13] for certain hypoeutectic binary solids of poly(ϵ-caprolactone) in trioxane. Similar epitaxial relationships were discovered between linear chain materials and other diluents including a number of aromatic compounds[14-17] (although phase diagrams were not determined), confirming earlier observations that specific molecular interactions occur in the crystallization of paraffin onto anthracene or phenanthrene.[18]

Although the epitaxial surface interactions have been very useful for preparation of oriented samples—e.g., for electron diffraction structure analysis[19-21]—or even as a probe of surface crystal structure,[22] the chain–diluent interactions have not been well characterized for all concentration domains in the (presumed) eutectic phase diagram. Indeed the type of interaction has been variously described. As stated above for some polymer–diluent crystallizations in excess of diluent, the interaction has been termed nonfaceted–faceted[10] where the diluent crystals exhibit faceted growth. Podolinskii et al.,[7] on the other hand, have characterized (structurally similar?) fatty acid–biphenyl eutectics as being totally anomalous. Certainly one complicating factor in dealing with polymer–diluent systems is that they are only "quasi-binary" due to the polydispersity of the polymer. Additionally the presence of chain folds will hinder polymer diffusion, as pointed out already by Smith and Pennings. We have therefore decided to study a series of well-defined binary solids composed of monodisperse molecular compounds in order to understand the mutual crystallographic interactions of these compounds in various concentration regions of the eutectic phase diagram if they exist. These molecular pairs are composed of the paraffin *n*-hexatriacontane and aromatics of the type investigated by Wittmann et al.,[14-16] to simulate polyethylene polymer–diluent interactions.

Materials and Methods

Chemicals and Specimen Preparation. The paraffin *n*-hexatriacontane used in this study, purchased from Aldrich Chemical Co. (Milawaukee, WI), is 98% pure and crystallized in the orthorhombic crystal form[23] either from solvent[24] or by epitaxial nucleation.[19] A series of related polynuclear aromatics, viz., naphthalene (purified) purchased from Mallinckrodt, Inc. (Paris, KY), anthracene (puriss) purchased from Fluka AG (Buchs, Switzerland), and acridine (purum), also from Fluka, were used as diluents because they have similar crystal structures and because they have different melting points and, in the case of melt-crystallized acridine II, different polarities. The crystal structures of naphthalene[25] and anthracene,[26] which have identical [001] packing[27] in the best-developed crystal face,[28] have been shown by Wittmann and Lotz[15] to epitaxially nucleate polymethylene chain packings in the same way. The interaction with acridine is unknown. Acridine II, although having a crystal structure[29] built up from molecular dimers, forms solid solutions with anthracene.[30] Another commonly used nucleating agent for paraffinic chains used in this study is benzoic acid[16] (ACS grade) purchased from Fisher Scientific (Fairlawn, NJ). As seen from its crystal structure,[31] the epitaxial nucleation of paraffin chains on the (001) surface is more anisotropic[16] than the polynuclear aromatics considered above. Thermodynamic data for these

0024-9297/89/2222-2169$01.50/0

Table I
Thermodynamic Data for Pure Compounds Used To Construct Binary Eutectic Solids

compound	T_m (peak value), °C	ΔH_f (obsd), cal/g	ΔH_f(lit.), cal/g
n-hexatriacontane (98%)	75.7	52.86	56.28[a]
naphthalene	81.1	31.94	35.06
anthracene	215.5	38.31	38.70
acridine	108.3	21.82	
benzoic acid	122.3	34.82	33.89

[a] Calculated value.[33]

materials determined in this laboratory by differential scanning calorimetry (DSC) are compared to literature values[32,33] for all cases except acridine, which is polymorphic, even when crystallized from the melt (Table I).

Samples used for the study of eutectic behavior were individually weighed on a Mettler AE163 five-place balance into aluminum DSC pans or another vessel after which they were fused together before determination of the melting point of the mixture after recooling. Samples for low-angle X-ray diffraction were scraped out of the reopened DSC pans and packed into the bottom of 1.0-mm-diameter thin glass capillary tubes by centrifugation. For polarized light microscopy fused samples were examined as a smear between two glass slides. Electron diffraction specimens were prepared by placing carbon-covered electron microscope grids over this smear, which was sandwiched between two mica plates. The specimen was heated to the melting point of the diluent and then recooled to room temperature as often described before.[34] Before electron diffraction studies, the diluent was sublimed away in vacuo.

Differential Scanning Calorimetry. DSC scans were carried out on 2–4-mg samples at various heating or cooling rates on a Mettler TA3300 instrument operated at maximum sensitivity. The temperature of the phase transitions is calibrated with a triple standard consisting of indium, lead, and zinc so that the temperature scale is fit as a polynominal that intersects the three known melting points. The transition enthalpy for an unknown material is compared to the known heat of fusion for indium.[35] For construction of binary phase diagrams we follow the convention of Smith and Pennings,[8] i.e., we plot the peak value of the lower melting component and the return temperature for the higher melting component endotherm. Only heating scans are used to construct the phase diagrams for reasons that will be made clear below.

X-ray Diffraction. X-ray diffraction measurements on bulk samples that had been cooled from the melt were made with a Rigaku rotating-anode X-ray generator with a Cu Kα source operated at 40 kV and 25 mA. The slit-collimated camera is homemade, and the detector is a TEC Model 205 position-sensitive proportional counter interfaced to a multichannel analyzer. Displays of the low-angle diffraction pattern on an IBM AT personal computer can be used to measure the interpeak spacings. The camera length is calibrated with the lamellar reflections from two known paraffin samples, viz., $C_{19}H_{40}$[36] and $C_{36}H_{74}$.[23]

Electron Diffraction. Selected area electron diffraction patterns from paraffin samples crystallized in the presence of different mole fractions of naphthalene or benzoic acid were obtained with a JEOL JEM-100B electron microscope equipped with a side-entry goniometer stage and operated at 100 kV. As usual,[37] care was taken to minimize radiation exposure to the specimen by use of low-beam currents and a fast photographic emulsion to record the diffraction pattern. Diffraction spacings were calibrated with a gold Debye–Scherrer pattern.

Polarizing Light Microscopy. Heated specimens were observed at a direct 200× magnification on a Leitz Ortholux light microscope with polarization optics, which is equipped with an automatic 35-mm camera. The heating and cooling scans were programmed on a FP80 controller for a Mettler FP800 thermosystem using samples held between glass slides in a FP82 hot stage.

Calculations

Calculation of the liquidus curve for a binary eutectic that is formed from the freezing of an ideal solution (or, if reversible, by melting of the solid) can utilize the well-known Schröder equations for freezing point depression, viz.

$$\ln x_1 = -\frac{\Delta H_{f_1}}{R}\left(\frac{1}{T} - \frac{1}{T_1}\right) \qquad (1)$$

$$\ln (1 - x_1) = -\frac{\Delta H_{f_2}}{R}\left(\frac{1}{T} - \frac{1}{T_2}\right)$$

where x_1 is the mole fraction of, e.g., the solvent, ΔH_{f_1} is the heat of fusion of the diluent, and T_1 is its melting temperature of the kelvin scale. A similar relation holds for the solute with mole fraction $x_2 = 1 - x_1$. The eutectic temperature and mole fraction can be found by solving the two equations for the desired unknown after setting $x_1 = x_e$ and $T = T_e$, where the subscript denotes the eutectic point.[2]

As has been long known,[38] there are cases when the molten solutions are far from ideal, e.g., when the solvent is somewhat polar and the solute is nonpolar or vice versa. In such a case the mole fraction is replaced by an activity a_i which is sometimes defined $a_i = x_i\gamma_i$, where γ_i is an activty coefficient.[38] An equation incorporating the effects of a nonzero heat of mixing due to nonequivalent intermolecular interactions has been derived by Lee.[39] The empirical interaction constant ρ_0, where $\Delta H_m = \rho_0 x_1 x_2$, is used to modify the ideal behavior stated above by the expression

$$\frac{\rho_0(1 - x_1)^2}{\Delta H_1} = \frac{T}{T^{ideal}} - 1 \qquad (2)$$

where the T^{ideal} was obtained from the Schröder equation (1). Alternatively lattice models such as the Flory–Huggins theory[40] are used, especially for polymer–diluent binary eutectics. The equations (1) above are modifed such that

$$\frac{1}{T} - \frac{1}{T_1} = \frac{R}{\Delta H_1}[\ln \phi_1 + 1 - \phi_1 + \chi(1 - \phi_1)^2]$$

$$\frac{1}{T} - \frac{1}{T_2} = \frac{R}{\Delta H_2}\frac{V_2}{V_1}[-\phi_1 + \chi\phi_1^2] \qquad (3)$$

The quantities are the same as before except that the subscript 1 specifically denotes the diluent that is supposed to have a higher melting point than the solute. Additionally ϕ_1 is a volume fraction and V_2 and V_1 are molar volumes of two constituents. (For polymers $V_2 = V_u$, the volume of a monomer unit.) The term χ accounts for nonequivalent interactions between molecular pairs in liquid solutions (similar to ρ_0 in (2)) which lead to nonideal behavior, e.g., the presence of directional (hydrogen bonding) interactions between ethanol molecules in mixtures with *p*-dibromobenzenes.[38] Implied here is another term in the entropy of mixing to account for deviations from Raoult's law behavior. Although the Flory–Huggins equation is often used to explain freezing points of polymer–diluent solutions, there is nothing in its formulation that states that it is only to be applied to polymer problems.[40] We use this lattice model as an alternate nonideal theory in this paper with the following assumptions: First, the molecular entities themselves are to occupy lattice sites whether they are linear chain or diluent species. Thus, there is no separate consideration of polymethylene chain repeat for the paraffins. Second, because the nonideal interactions between lattice sites are polar or hydrogen bonding in nature and not the covalent linkage between

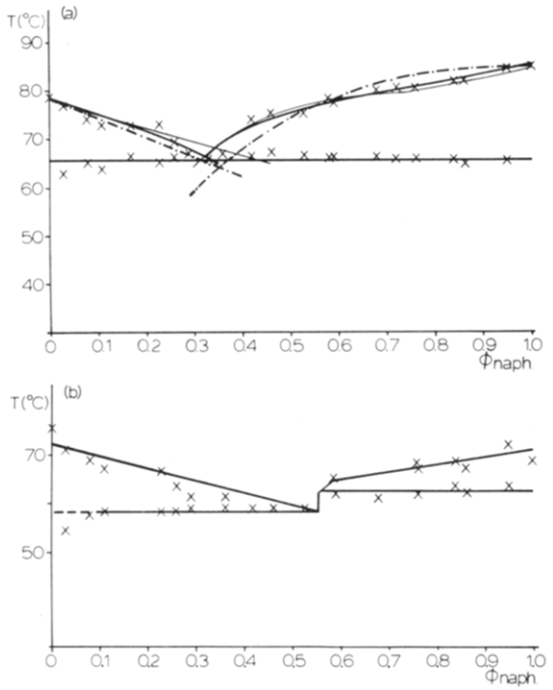

Figure 1. (a) Binary phase diagram for *n*-hexatriacontane in naphthalene. The experimental liquidus curves are very close to the melting curves predicted from ideal theory (thin solid line). A calculation of the liquidus curves with the lattice model in eq 3 (dashed line) also gives a fairly good approximation to the experimental curves when the interaction term $\chi = 0$. (b) The phase diagram drawn from cooling curves is somewhat different. Aside from consistent undercooling, the eutectic point is shifted somewhat toward the naphthalene-rich side. (Although experimental transition temperatures are used to determine the eutectic composition, one could also employ Tammann's method[50] based on a plot of transition enthalpies.)

chain repeats, it is expected that the values of χ will not have the specific significance ordinarily assigned to them in polymer science. It is important to realize that we are only concerned with a deviation from Raoult's law behavior which occurs when the molecular volumes are dissimilar and $\chi \neq 0$. Because of the somewhat different use of eq 3 from its ordinary application to polymer/diluent systems, we designate it as the "lattice model" in the paper.

Results

Naphthalene–*n*-$C_{36}H_{74}$. The eutectic phase diagram for binary solids formed from naphthalene and *n*-hexatriacontane, which is constructed from DSC endotherms, is shown in Figure 1a. From the intersection of liquidus and solidus curves, the eutectic point is observed at $\phi_e = 0.33$; the measured eutectic temperature is $T_e = 66$ °C. Calculations of liquidus curves based on the ideal Schröder equation (1) produce a close match to the observed values (Figure 1a) with a eutectic composition predicted at $\phi_e = 0.345$ and a eutectic isotherm near $T_e = 68$ °C (Note that the original calculations based on ideal theory were made in terms of mole fractions, but later these are converted to volume fractions for facile comparison to calculations based on eq 3. This change in units will also be applied below.) The lattice model, eq 3, produces similar results when the interaction parameter $\chi = 0$, i.e., $\phi_e = 0.36$, $T_e = 64$ °C. The cooling curve for the binary melt somewhat resembles the phase diagram constructed from heating scans, except that there is a more or less consistent undercooling of the melt before crystallization, the most pronounced undercooling seen for higher concentrations of the diluent, as found also by Smith and Pennings[11]

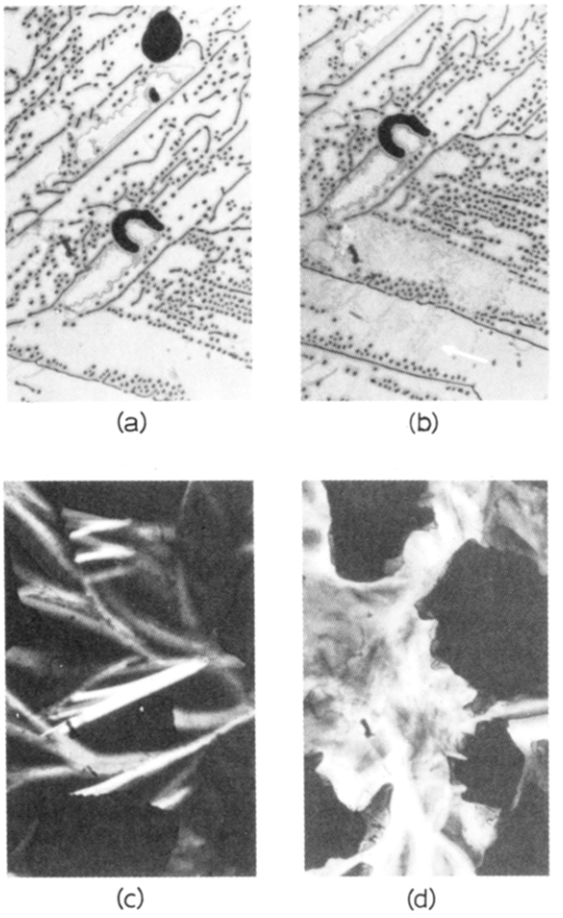

Figure 2. Observations of *n*-hexatriacontane–naphthalene crystallization from the melt in a polarizing light microscope (refer to Figure 1b). At high concentrations of naphthalene (e.g., $\phi = 0.90$), platelike layers of the aromatic crystallizes first as in (a) and an overgrowth of paraffin is deposited when the eutectic solidus is reached as in (b) (e.g., arrow). At high concentrations of the paraffin (e.g., $\phi_1 = 0.10$), needlelike crystals of paraffin appear first from the melt as in (c), and intercrystalline spaces are then filled in by the eutectic solid (d). In the former example (b) the paraffin–naphthalene interaction is epitaxial, but in the latter (d) the interaction is nonspecific.

(Figure 1b). The eutectic point is shifted, however, to $\phi_e \simeq 0.54$, and there appears to be a temperature shift for the solidus line on either side of the eutectic similar to the case found for isotectic polypropylene in pentaerithrityl tetrabromide.[12]

Although it was not possible to obtain as clear a demonstration of the total phase separation in naphthalene–*n*-$C_{36}H_{74}$ binary solids by low-angle X-ray diffraction (due to the limited angular detector range used in the experiment) as is shown below for anthracene–*n*-$C_{36}H_{74}$, detection of the low-angle reflections from the paraffin component at the same angular position over all concentrations certainly demonstrates that no partial solubility is to be found. Moreover, with principles stated by Kitaigorodsky[41] for solid solution formation, there is no reason to expect significant solid solubility for such dissimilar molecules, as seen already by the phase diagram in Figure 1a. A study of the crystal growth from cooled melts by optical microscopy, on the other hand, reveals a clear distinction between the two regions of the phase diagram on respective sides of the eutectic point. On the aromatic-rich side, the naphthalene crystallizes first (as expected) as large platelets (Figure 2a). When the eutectic solidus line is reached, the paraffin component crystallizes as an overlayer (Figure 2b). As shown by Wittmann and Manley,[14]

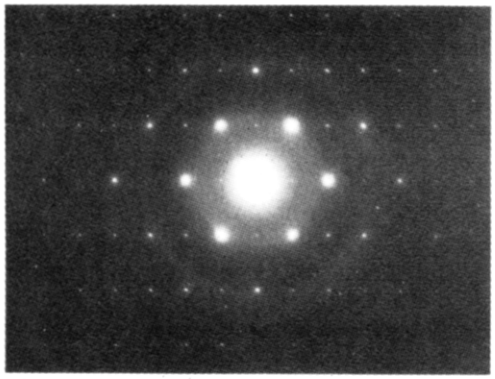

(a)

(b)

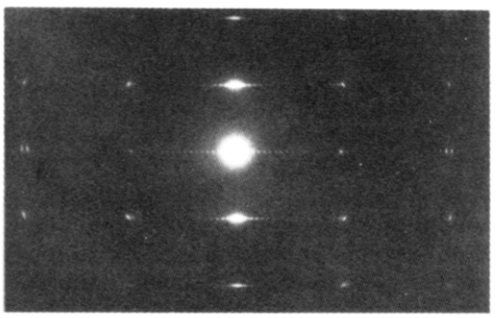

(c)

Figure 3. Electron diffraction patterns from *n*-hexatriacontane crystallized in the presence of naphthalene. (a) At the left of the eutectic point, only the usual melt crystallization of paraffin is found with chain axes perpendicular to the best-developed crystal face, as shown by the *hk*0 diffraction pattern. (b) At the right of the eutectic point in Figure 1a, epitaxially oriented paraffin crystals where chain axes lie parallel to the major crystal face can always be found, as shown by the characteristic 0*kl* diffraction patterns. (c) When these crystals are tilted 34° around *c** the *hhl* pattern can also be obtained.

the relationship between the two crystal surfaces is epitaxial so that the (100) plane of the paraffin crystals align along ⟨110⟩ directions on the naphthalene (001) face, an interaction directed by lattice matching. We have obtained electron diffraction patterns over all concentrations from crystals that were formed after thin films of naphthalene–*n*-$C_{36}H_{74}$ were melted in the presence of carbon-covered electron microscope grids. Epitaxial orientation of the paraffin, so that its long axes parallel the naphthalene (001) face, occurs only at aromatic concentrations above the eutectic point (Figure 3b). On the paraffin-rich side one sees only the usual melt crystallization of paraffin (Figure 3a). By light microscopy the paraffin-rich solid is found to involve mainly lateral intermixing of the two molecular species (Figure 2c,d), without specific epitaxial relationships between the two components.

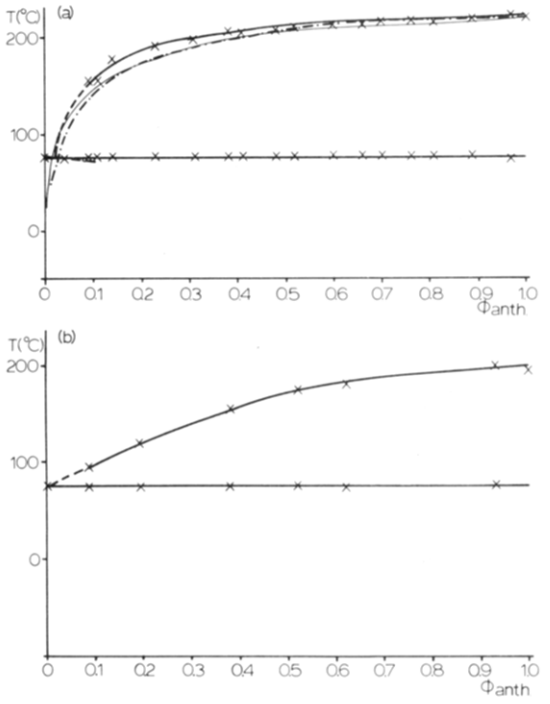

Figure 4. (a) Binary phase diagram for *n*-hexatriacontane in anthracene. Although the crystal structures of naphthalene and anthracene are very similar, this phase diagram has a eutectic point near the pure paraffin concentration due to the greater difference in paraffin and diluent melting points. Both Schröder (thin solid line) and the lattice theory (dashed line) equations match the experimented liquidus curve well. (b) Aside from a consistent undercooling of the anthracene liquidus curve, the phase diagram drawn from DSC cooling scans is very similar to the one drawn from heating scans (a) and is rather independent of cooling rate.

Anthracene–*n*-$C_{36}H_{74}$. Although anthracene and naphthalene have similar crystal structures,[27] the phase behavior of the former with *n*-$C_{36}H_{74}$ (Figure 4a) is unlike the eutectic diagram in Figure 1a in that the eutectic point lies very close to the pure paraffin composition. Calculation of the liquidus curve using either ideal theory or the lattice model with $\chi = 0$ reproduces the experimental curve reasonably well. The eutectic point occurs at $\phi_e \simeq 0.02$, and the solidus isotherm is found at $T_e = 75$ °C, also in reasonable agreement with the model calculations. Cooling curves (Figure 4b) reveal that the undercooling for anthracene crystallization is a smooth function of the binary liquid concentration, independent of cooling rate.

The crystalline separation of anthracene from *n*-$C_{36}H_{74}$ in the solid state is found by low-angle X-ray diffraction (Figure 5a). Observation of crystallization behavior in the light microscope clearly shows that the higher melting anthracene component first forms faceted crystals from the melt (Figure 6a,c) after which the paraffin crystallizes as an overgrowth (similar to the case with naphthalene-rich eutectics with paraffin[15]) and, additionally, as interstitial laths with perpendicular chain orientation (Figure 6b,d). By electron diffraction Wittmann and Lotz[15] have shown that the overgrowth of the paraffin onto the anthracene crystal face is epitaxial. This is expected since the naphthalene and anthracene crystal structures are homologous.[27]

Acridine–*n*-$C_{36}H_{74}$. The experimental phase diagram of acridine with *n*-hexatriacontane (Figure 7) strongly resembles the eutectic found with anthracene–*n*-$C_{36}H_{74}$, with a projected eutectic point occurring near $\phi_e = 0.02$ and a eutectic isotherm at $T_e = 74.5$ °C. Calculation of the liquidus line by ideal theory is not successful in pre-

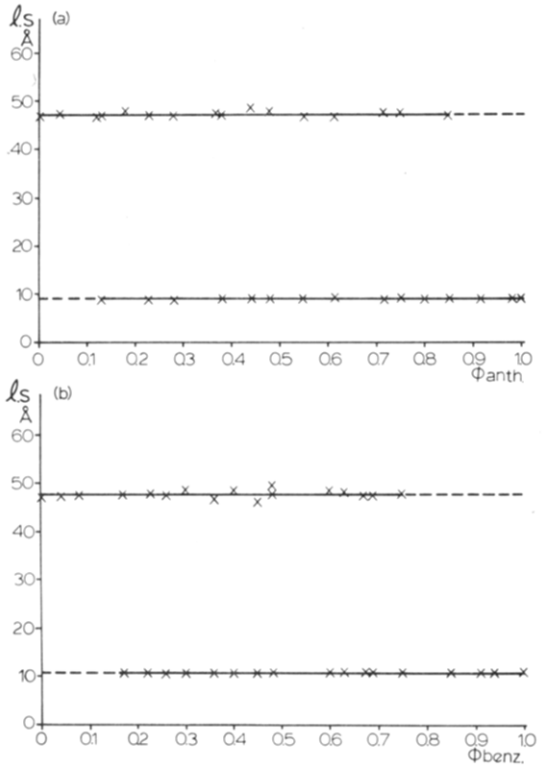

Figure 5. Low-angle X-ray diffraction spacing from paraffin–diluent solids: (a) *n*-hexatriacontane–anthracene; (b) *n*-hexatriacontane–benzoic acid. From the constancy of these spacings of eutectic solids appear to contain rather large crystals of pure components which remain separated over the whole concentration range.

dicting the eutectic concentration (Figure 7). Nonideal theory is only slightly more successful; for example, a model based on the lattice model with $\chi = 0.6$ at least produces a reasonably close fit to the solidus temperature, but the eutectic concentration is still far from its measured value. From eq 2 the eutectic point can be reproduced when $\rho_0 = 1.15$ kcal/mol, but the match to the liquidus curve is poor. Cooling curves for acridine–*n*-$C_{36}H_{74}$ melts are interesting in that the crystallization temperature dependence on melt concentration includes several minima. A complete description of the phase diagram based on cooling curves has been provided by Prof. P. Phillips et al. (personal communication) and is forthcoming.

As shown by the isotherm in Figure 7 at 103 °C, acridine crystallizes in several polymorphic forms, the acridine II form obtained from the melt being most like the crystal structure of anthracene although the molecules are closely associated as dimers.[30] Thus, because of uncertainities in what crystal polymorphs are involved in the paraffin–aromatic interaction, no low-angle X-ray diffraction data were obtained from this complex system; likewise, the crystallization behavior from the melt was not studied by light microscopy.

Benzoic Acid–*n*-$C_{36}H_{74}$. The phase diagram of benzoic acid with *n*-hexatriacontane is depicted in Figure 8a. The measured eutectic is near $\phi_e = 0.07$ and the isotherm at $T_e = 75.5$ °C. As found also for binary mixtures of the paraffin with acridine, the Schröder equation does not explain the melting behavior of these solids. The lattice model is hardly more successful than ideal theory, even when the interaction term is as large as $\chi = 1.0$. The regular solution theory (eq 2) is most successful (Figure 8a) when the interaction parameter $\rho_0 = 0.700$ kcal/mol is chosen, a value comparable to those used to simulate nonideal lipid-phase diagrams.[39]

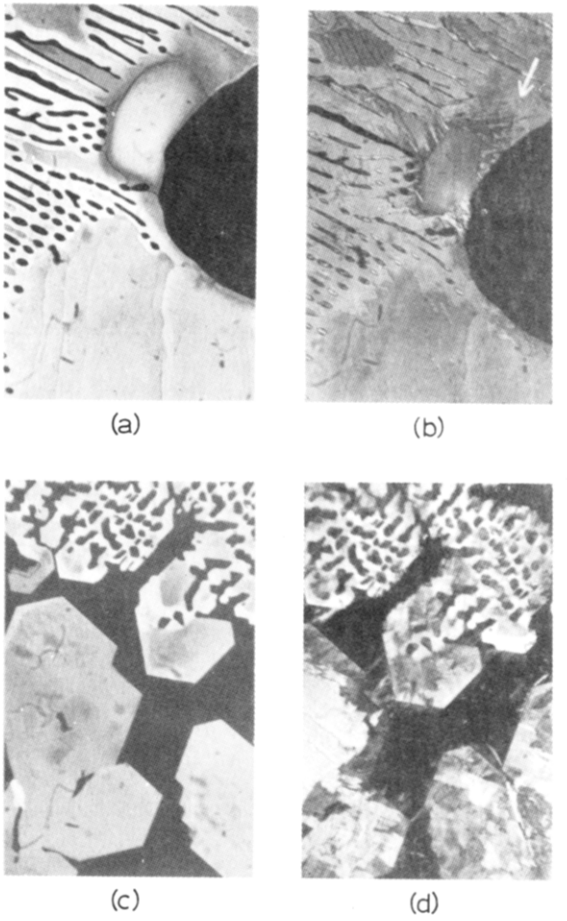

Figure 6. Observation of *n*-hexatriacontane–anthracene crystallization from the melt in a polarizing light microscope (refer to Figure 4b). At nearly all concentrations of anthracene, some epitaxial overgrowth of the paraffin is found, consistent with the phase diagram. For example, at $\phi_1 = 0.90$ the crystallization of anthracene from the melt near 190 °C (a) is followed by a lathlike overgrowth of the paraffin after the eutectic solidus line is crossed, e.g., at 65 °C (see arrow) (b). At the other end of the concentration scale, e.g., at $\phi = 0.10$, the anthracene crystallization monitored at 80 °C (c) is followed by paraffin crystallization, e.g., at 55 °C (d). Since the paraffin concentration is higher, both specific epitaxial overgrowths and nonspecific crystallization between anthracene crystals are seen.

Low-angle X-ray diffraction can be used to demonstrate the separate crystallization of the two components from the melt (Figure 5b). Cooling curves, on the other hand, reveal (Figure 8b) that the initial crystallization of benzoic acid from the melt does not occur at uniform undercoolings over the whole orientation range. There may be some slight dependence of the amount of undercooling on cooling rate.

Benzoic acid crystallizes in two habits, one platelike and the other acicular.[28] Light microscopic observations (Figure 9) demonstrate that after initial crystallization of benzoic acid from the melt, the paraffin can crystallize either on these plates or between them for all concentrations. In the former case the relationship is epitaxial as shown before[16] with the (001) face of benzoic acid nucleating the (100) zone of the *n*-paraffin; in the latter instance the paraffin grows with chains perpendicular to the support surface. Electron diffraction patterns from the two crystal orientations are like those shown in Figure 3.

Discussion

To explain deviation from Raoult's law in the formation of regular solutions, e.g., in a binary melt, two factors can

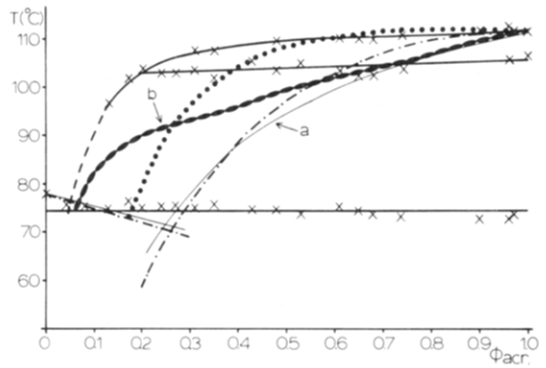

Figure 7. Phase diagram of *n*-hexatriacontane in acridine. The observed eutectic behavior is similar to the case of anthracene. Note the isotherm above the eutectic solidus, which denotes a polymorphic phase transition for the diluent. Neither the Schröder equation (curve marked a) nor the lattice model (dashed and dotted lines) accounts for the observed phase diagram, not even when rather large molecular interaction constants χ are used (maximum value $\chi = 0.6$). The nonideal correction proposed by Lee[39] (curve marked b) is most successful in finding the eutectic point and solidus temperature when $\rho_0 = 1.15$ kcal/mol, but the theoretical curve is not very close to the observed liquidus.

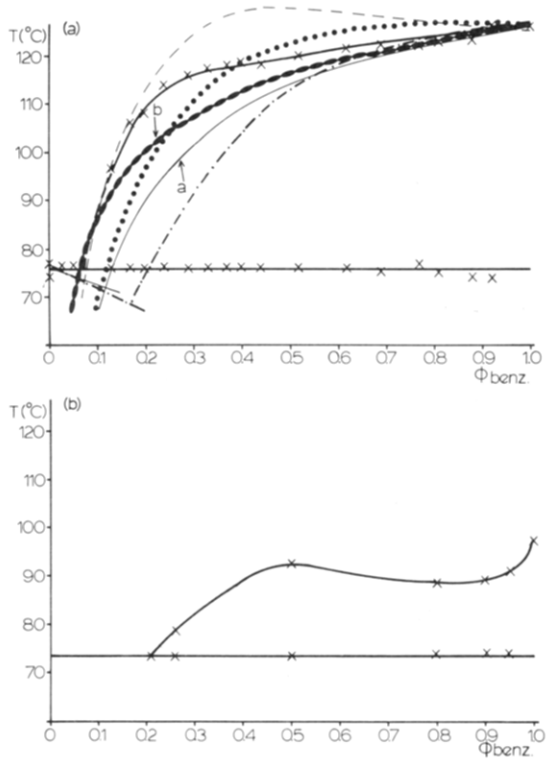

Figure 8. (a) Phase diagrams of *n*-hexatriacontane and benzoic acid. Neither the Schröder equation (thin solid curve marked a) nor the lattice model (three broken curves) give close matches to the observed phase diagram, even when the latter nonideal theory incorporates a molecular interaction term as large as $\chi = 1.0$. The best match to the observed liquidus is found when Lee's correction to the Schröder equation (curved labeled b) is used where $\rho_0 = 0.7$ kcal/mol. (b) Cooling curves for paraffin–benzoic acid melts reveal that the undercooling for benzoic acid crystallization is not uniform for the concentration series.

be thought of to contribute to nonideal behavior, viz., unequal molecular sizes and specific molecular interactions. Although no suitable quantitative theory that will explain these nonideal deviations is available, Pitzer and Brewer[38] have discussed the theoretical approach used by various workers in the field. In this paper, we have employed the lattice theory[40] first, mainly because it both contains a convenient term χ to treat unlike molecular interactions

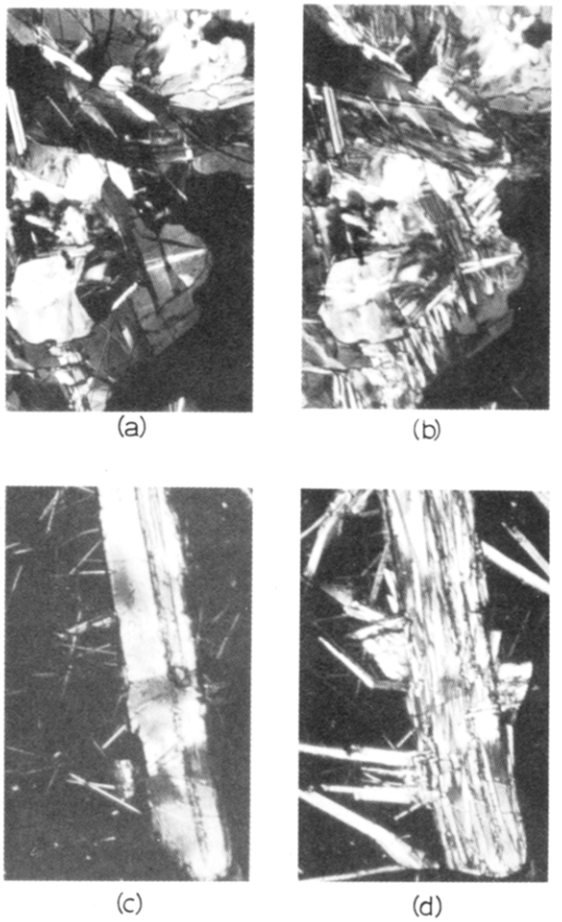

Figure 9. Observation of *n*-hexatriacontane–benzoic acid crystallization from the melt in the polarizing light microscope. At high benzoic acid concentration, e.g., $\phi = 0.90$, both plate and acicular crystals grow from the melt (a). When the eutectic solidus is reached, numerous lathlike paraffin crystal overgrowths can be seen. (b) At lower concentrations of benzoic acid, e.g., $\phi_1 = 0.21$, after growth of the benzoic acid crystals from the melt (c), both epitaxial overgrowth and nonspecific interstitial growths of the paraffin can be found when the solidus line is reached (d).

and includes the effect of different molecular volumes in the definition of activity.

In the above phase diagrams of paraffin–diluent compositions, for which only van der Waals interactions are expected to be predominant (i.e., for naphthalene and anthracene), it is seen that either the Schröder equation or the lattice model equations, where $\chi = 0$, will give reasonably good fits to the experimental points for the liquidus curve and also predict the solidus temperature and eutectic composition. The situation is quite different when the diluent is either acridine or benzoic acid. In neither case is ideal theory adequate to explain the liquidus curve. The lattice model is scarcely more satisfactory. That molecular interactions may be an important factor in this grossly nonideal behavior is consistent with previous experience.[38] Benzoic acid is known to associate in hydrogen-bonded dimers,[31] a factor that will affect the entropy of mixing in a solution in a way somewhat similar to the constraints imposed to free mixing by covalent links in a polymer chain. Nevertheless, the nonideal formulation of Lee[39] produces a better match to the observed phase diagram. The sign of the correction factor ρ_0 is significant since it signifies a stronger molecular self-interaction in pure components than cross interactions between the two compounds in the eutectic.[42] While the crystal packing of acridine can be somewhat similar to that of anthracene,[29] there is also evidence that the molecular associations are

tighter than expected for a van der Waals molecule, to the extent that the group thermal motion occurs in a molecular dimer. Specific molecular interactions may also be indicated by the nonsmooth appearance of cooling curves for melts containing these polar molecules. A more accurate phase diagram for acridine–polymethylene has been obtained from DSC cooling scans and contains similar features.[43] Although the description of nonideal behavior is somewhat qualitative, it is not probably appropriate here to consider other factors such as the concentration dependence of the interaction parameter χ to account for the nonideal solubility of the paraffin with its diluent in the comelt in order to avoid too many parameters in the model. Neither nonideal theory matches the phase diagram very well, perhaps due to the polymorphism of the diluent.

Of principle interest in this study are the interfacial interactions involved in the formation of paraffin–diluent eutectic solids. X-ray diffraction measurements of such binary solids indicate that the components are phase separated as large individual crystals rather than some sort of lamellar superlattice. A similar conclusion might be drawn initially from the light micrographs obtained from crystallized binary melts, in which the diluent in the aromatic-rich melt always solidifies first as a faceted crystal. As shown above and in previous work, careful observation, however, reveals an epitaxial relationship can exist between crystalline plates when paraffin crystallizes onto the diluent. A less specific interaction occurs when the paraffin crystallizes between diluent crystals—e.g., in a low diluent concentration range (in the case of naphthalene) or when two diluent crystal habits occur (e.g., benzoic acid). With the nomenclature of Hunt and Jackson,[4] then, eutectic crystallization can be either the faceted–nonfaceted or the faceted–faceted type. In the former, cooperative growth, the molecular interaction can be explained by specific lattice matchings as described by Wittmann and coworkers.[14,16] Specifically, the diluents naphthalene (or anthracene) and benzoic acid crystallize such that the major (001) faces are also those that are atomically flattest in terms of surface packing but that also contain intermolecular grooves between the outermost atoms that match the side-to-side packing distance of paraffin chains.[14,16] Other boundary crystal faces (as drawn, e.g., by Winchell[28]) are not so flat and do not match any spacing of the paraffin crystal packing; this interaction is therefore nonepitaxial.

In light of the importance attached to epitaxial relationships for metallic lamellar eutectics,[3] it is important to stress their general importance in organic lamellar eutectics as well. Certainly for the low paraffin concentration regions of the binary solids considered here, the only factor that prevents growth of a lamellar eutectic is the difference in melting points and/or preferred habit of the first crystallizing component—indeed, strictly speaking, the cooperatively crystallized solids considered here are a trivial case of the lamellar eutectic in which only two layers are permitted. Since the layer relationship depends upon a sequence of crystal growth, the epitaxy can only be the faceted–nonfaceted type. On the other hand, exact epitaxial relationships between methyl end planes were found to be very important for paraffin eutectic solids,[44] not only in forming the lamellar superlattice structure of the eutectic solid itself but also in its orientation with pure domains of the higher melting component. Due to the similarity of materials, the interactions are nonfaceted–nonfaceted. It would also be worthwhile to consider Podolinskii's[6,7] observations on interfacial interactions between organic crystals in terms of epitaxy, since, for example,

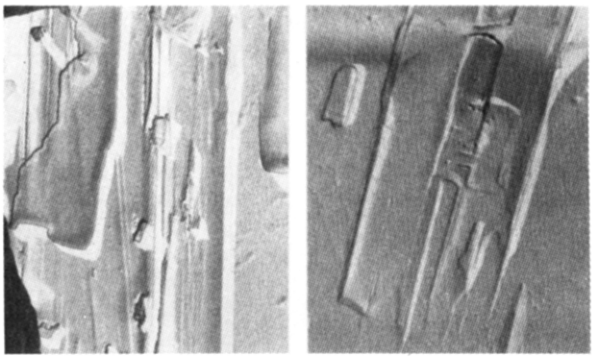

Figure 10. Probably due to mismatch between the surface lattice spacings of paraffin and an interesting organic substrate, the epitaxially crystallized crystals are curvilinearly deformed. This can be demonstrated by C–Pt shadowed laths of *n*-hexatriacontane epitaxially crystallized on benzoic acid, e.g., by the concave appearance of such lath crystals in (a) and (b).

unobserved faceted–nonfaceted interactions may lead to a specific epitaxial orientation of lauric acid on biphenyl,[7] since this material can orient polymethylene chains[15] packing in the $0_\perp$ methylene subcell characteristic of the fatty acid crystal structure.[46]

Another aspect of the epitaxial interaction across crystal interfaces by lattice matching is the distortion caused by small lattice differences. Kerr and Lewis[3] proposed a model for relief of accumulated mismatch in lamellar alloys in which an overlayer is buckled occasionally so that most of the crystal can fit on the nucleating layer. Fryer[47] has demonstrated the presence of lattice imperfections in phthalocyanines epitaxially oriented on cleaved salt crystals which are caused by similar mismatches. For the two major materials used in this laboratory to orient polymethylene chain lattices, i.e., naphthalene and benzoic acid, the mismatches involved for nucleating the (100) zone of orthorhombic paraffin (such as *n*-hexatriacontane) are 2.3 and 3.6%, respectively. The effect of such mismatches is shown in Figure 10, in which the epitaxially oriented paraffin laths are shown to have much more pronounced curvilinear distortions than found for samples crystallized from solution onto a carbon grid.[48] Recent experiments in this laboratory (H. Hu and W. P. Zhang, unpublished data) indicate that these distortions can be minimized by annealing the paraffin in the presence of the nucleating underlayer, presumably to achieve a closer match of the two lattice spacings at a suitable temperature.

Even with such difficulties, it should be stated that epitaxial relationships between linear chain molecules and aromatic diluents of the type described here have done much to advance the electron diffraction and electron microscopic study of polyethylene and other linear molecules. It has permitted orientation of these materials so that the electron beam projects along a suitably short unit cell axis to minimize diffraction intensity distortions due to crystal curvature. Quantitative crystal structure analysis that describe the entire unit cell contents are permitted, unlike the case for data from solution crystallized samples, from which only a partial analysis is often possible. Already this has led to the examination of linear polymers, phospholipids, and cholesteryl esters, in addition to paraffins not only in their "pure" form but also as mixtures and in a study of their thermotropic behavior to obtain a less ambiguous view of structural features in the most optimal projection onto the chain axis.[49]

Acknowledgment. Research described here was supported by a grant from the National Science Foundation (DMR 86-10783). We are grateful to Prof. Paul Phillips for showing us preliminary data from his work on the polyethylene–acridine solids.

Registry No. Hexatriacontane, 630-06-8; naphthalene, 91-20-3; anthracene, 120-12-7; acridine, 260-94-6; benzoic acid, 65-85-0.

References and Notes

(1) Copley, G. N. *J. Chem. Educ.* **1959**, *36*, 596.
(2) Hsu, E. C.-H.; Johnson, J. F. *Mol. Cryst. Liq. Cryst.* **1974**, *27*, 95.
(3) Kerr, H. W.; Lewis, M. H. *Advances in Epitaxy and Endotaxy*; Schneider, H. G., Ruth, V., Eds.; Verlag: Leipzig, 1971; pp 147–164.
(4) Hunt, J. D.; Jackson, K. A. *Trans. Metall. Soc. AIME* **1966**, *236*, 843.
(5) Jackson, K. A.; Hunt, J. D. *Trans Metall. Soc. AIME* **1966**, *236*, 1129.
(6) Podolinskii, V. V. *Dokl. Akad. Nauk. SSSR* **1980**, *254*, 1168.
(7) Podolinskii, V. V.; Taran, Y. N.; Drykin, V. G. *Sov. Phys.—Crystallogr. (Engl. Transl.)* **1987**, *32*, 588.
(8) Smith, P.; Pennings, A. J. *Polymer* **1974**, *15*, 413.
(9) Pennings, A. J.; Smith, P. *Br. Polym. J.* **1975**, *7*, 460.
(10) Smith, P.; Pennings, A. J. *J. Mater. Sci.* **1976**, *11*, 1450.
(11) Smith, P.; van Ekenstein, G. O. R. A.; Pennings, A. J. *Br. Polym. J.* **1977**, *9*, 258.
(12) Smith, P.; Pennings, A. J. *J. Polym. Sci., Polym. Phys. Ed.* **1977**, *15*, 513.
(13) Wittmann, J. C.; Manley, R. St. J. *J. Polym. Sci., Polym. Phys. Ed.* **1977**, *15*, 1089.
(14) Wittmann, J. C.; Manley, R. St. J. *J. Polym. Sci., Polym. Phys. Ed.* **1978**, *16*, 1891.
(15) Wittmann, J. C.; Lotz, B. *J. Polym. Sci., Polym. Phys. Ed.* **1981**, *19*, 1837, 1853.
(16) Wittmann, J. C.; Hodge, A. M.; Lotz, B. *J. Polym. Sci., Polym. Phys. Ed.* **1983**, *21*, 2495.
(17) Dorset, D. L.; Pangborn, W. A.; Hancock, A. J. *J. Biochem. Biophys. Methods* **1983**, *8*, 29.
(18) Willems, J. *Naturwissenschaften* **1955**, *42*, 176.
(19) Moss, B.; Dorset, D. L.; Wittmann, J. C.; Lotz, B. *J. Polym. Sci., Polym. Phys. Ed.* **1984**, *22*, 1919.
(20) Dorset, D. L. *J. Polym. Sci., Polym. Phys. Ed.* **1986**, *24*, 79.
(21) Dorset, D. L. *Biochim. Biophys. Acta* **1988**, *938*, 279.
(22) Wittmann, J. C.; Lotz, B. *J. Polym. Sci., Polym. Phys. Ed.* **1985**, *23*, 205.
(23) Teare, P. W. *Acta Crystallogr.* **1959**, *12*, 294.
(24) Dorset, D. L. *Acta Crystallogr.* **1976**, *A32*, 207.
(25) Cruickshank, D. W. J. *Acta Crystallogr.* **1957**, *10*, 504.
(26) Sinclair, V. C.; Robertson, J. M.; Mathieson, A. M. L. *Acta Crystallogr.* **1950**, *3*, 245, 251.
(27) Kitaigorodsky, A. I. *Molecular Crystals and Molecules*; Academic Press: New York, 1973; pp 40–41, 108–110.
(28) Winchell, A. N. *The Optical Properties of Organic Compounds*; Academic Press: New York, 1954.
(29) Phillips, D. C.; Ahmed, F. R.; Barnes, W. H. *Acta Crystallogr.* **1960**, *13*, 365.
(30) Miasnikova, R. M.; Kitaigorodskii, A. I. *Sov. Phys.—Crystallogr. (Engl. Transl.)* **1958**, *3*, 157.
(31) Sim, G. A.; Robertson, J. M.; Goodwin, T. H. *Acta Crystallogr.* **1955**, *8*, 157.
(32) Weast, R. C., Ed. *CRC Handbook of Chemistry Physics*, 60th ed.; CRC Press: Boca Raton, FL, 1987; pp C724–726.
(33) Dollhopf, W.; Grossmann, H. P.; Leute, U. *Colloid Polym. Sci.* **1981**, *259*, 267.
(34) Dorset, D. L. *J. Electron Microsc. Tech.* **1987**, *7*, 35.
(35) Wendlandt, W. W. *Thermal Analysis*, 3rd ed.; Wiley: New York, 1986; p 276.
(36) Nyburg, S. C.; Potworowski, J. A. *Acta Crystallogr.* **1973**, *B29*, 347.
(37) Dorset, D. L. *J. Electron Microsc. Tech.* **1985**, *2*, 89.
(38) Lewis, G. N.; Randall, M. *Thermodynamics*, 2nd rev. ed.; Pitzer, K. S., Brewer, L., Eds.; McGraw-Hill: New York, 1961; pp 227–230, 280–296.
(39) Lee, A. G. *Biochem. Biophys. Acta* **1978**, *507*, 433.
(40) Flory, P. J. *Principles of Polymer Chemistry*; Cornell University Press: Ithaca, NY, 1953; pp 507–511, 568–571.
(41) Kitaigorodsky, A. I. *Mixed Crystals*; Springer-Verlag: Berlin, 1984; pp 200 ff.
(42) Koynova, R. D.; Kuttenreich, H. L.; Tenchov, B. G.; Hinz, H.-J. *Biochemistry* **1988**, *27*, 4612.
(43) Dibrell, F. S.; Phillips, P. J. *Bull. Am. Phys. Soc.* **1988**, *33*(3), 589.
(44) Dorset, D. L. *Macromolecules* **1986**, *19*, 2965.
(45) Abrahamsson, S.; Dahlén, B.; Löfgren, H.; Pascher, I. *Prog. Chem. Fats Other Lipids* **1978**, *16*, 125.
(46) Sydow, E. v. *Ark. Kemi* **1956**, *9*, 231.
(47) Fryer, J. R. *J. Electron Microsc. Tech.*, in press.
(48) Dorset, D. L. *Acta Crystallogr.* **1980**, *A36*, 592.
(49) Dorset, D. L. *J. Electron Microsc. Tech.*, in press.
(50) Tammann, G. *A Text Book of Metallography*; Dean, R. G., Swenson, L. G., Translators, Chemical Catalog: New York, 1925; pp 178–179.

Kinetic–Mechanistic Studies on the Photorearrangement of *o*-Nitrobenzyl Ester Groups in Polymer Matrices

W. K. Wong,† H. Schupp,‡ and W. Schnabel*,†

Hahn-Meitner-Institut Berlin GmbH, Bereich Strahlenchemie, D-1000 Berlin 39, FRG, and BASF AG, D-6700 Ludwigshafen, FRG. *Received May 27, 1988*

ABSTRACT: Films of copolymers containing 5 mol % *o*-nitro-α-methylbenzyl acrylate and methyl methacrylate, butyl methacrylate, or butyl acrylate in various combinations were subjected to flash photolysis (λ_{inc} 347 or 355 nm; flash length, 25 ns or 100 ps, respectively) at temperatures between 77 and 473 K. Nitronic acid was formed as an intermediate at all temperatures via two routes: a very fast singlet route with a lifetime $\tau < 200$ ps and a "slow" triplet route conforming to first-order kinetics. The temperature dependence of both the nitronic acid yield and the rate constant of the slow formation process reflected changes in the physical state of the matrix connected with the onset of side group rotations and the glass transition. The decay of the nitronic acid groups was nonexponential at temperatures up to 450 K, i.e., even at temperatures above T_g. The decay of the optical density (OD) of nitronic acid conformed to the relationship $OD_t = OD_0 \exp(-\alpha t^\beta)$ with $\beta = 0.5$. The kinetic matrix effect is discussed with respect to dispersive reaction kinetics and the free volume concept. At temperatures above 450 K, the nitronic acid decay followed first-order kinetics, indicating that local displacements and size variations of free volume elements were no longer the rate-determining process.

Introduction

The mechanism and the kinetics of the photorearrangement of *o*-nitrobenzyl esters in solution were the objective of recent studies,[1,2] which led to the mechanism illustrated in Scheme I. Notably, the rearrangement involves a rather long-lived intermediate, nitronic acid, which has a strong optical absorption band around $\lambda = 400$ nm. The quantum yields of bond cleavage in the photorearrangement, ϕ(PR), were found to be significantly influenced by the substituent R^1 in the α-position and to be

† Hahn-Meitner-Institut Berlin GmbH.
‡ BASF AG.